Theor Chem Acc (2011) 128:393–404
DOI 10.1007/s00214-010-0820-9

REGULAR ARTICLE

Current trends in the computational modelling of polyoxometalates

Xavier López · Pere Miró · Jorge J. Carbó · Antonio Rodríguez-Fortea · Carles Bo · Josep M. Poblet

Received: 9 July 2010 / Accepted: 10 September 2010 / Published online: 28 September 2010

Abstract Computational chemistry applied to the study of polyoxometalates has achieved its maturity in the last years. During two decades, important advances have been made using theoretical tools in the comprehension and interpretation of many relevant issues. In the present mini-review, we want to stress that different techniques have been incorporated to the routine of computation: from the very first Hartree–Fock LCAO-SCF calculation on the decavanadate anion, followed by numerous density functional theory–based studies on increasingly complex systems, also applying correlated ab initio techniques for magnetism and, more recently, using molecular dynamics to analyse properties in liquid media, the information provided by computational chemistry gets more and more relevant.

Keywords Polyoxometalates · Computational chemistry · Inorganic chemistry · DFT · Molecular dynamics · Car-Parrinello method

Published as part of the special issue celebrating theoretical and computational chemistry in Spain.

Dedicated to the memory of Marie-Madeleine Rohmer (1946–2010).

X. López · J. J. Carbó · A. Rodríguez-Fortea · C. Bo · J. M. Poblet (✉)
Departament de Química Física i Inorgànica, Universitat Rovira i Virgili, Marcel·lí Domingo s/n, 43007 Tarragona, Spain
e-mail: josepmaria.poblet@urv.cat

P. Miró · C. Bo (✉)
Institut Català d'Investigació Química (ICIQ), Av. Països Catalans 16, 43007 Tarragona, Spain
e-mail: cbo@ICIQ.es

1 Introduction

Polyoxometalates [1–4] (POMs), a rapidly growing family of polynuclear metal oxide molecular anions, congregates a huge number of compounds that display wide diversity both in composition and in shape. Main transition metals present in POMs, W and Mo (V and Nb to a lesser extent) in their highest oxidation states, together with bridging and terminal oxygens, build up the POM framework. The basic octahedral MO_6 and square pyramidal MO_5 units share either vertices or edges and, under the influence or not of some templating species, condense and grow larger clusters. With the exception of some few, almost all the elements have been incorporated either in the POM structure itself or encapsulated within. This rather simplistic definition holds, however, for an enormous variety of structures ranging from small molecules to supramolecular nano-sized aggregates displaying high symmetry in most cases. POMs are unique from several viewpoints, and their chemical and structural possibilities have still unseen limits. Regular shapes resembling balls, cylinders and wheels, as well as displaying channels or cavities have been reported [5–8]. The size and shape of a POM can be purposely designed depending on the pH and the temperature conditions, the ionic strength or the presence of additional ligands during the synthesis, among other variables [4, 9]. Their amazingly vast structural diversity has derived into exciting applications in fields as diverse as medicine, magnetism and catalysis to cite just a few [10–13]. From the first reports in the early nineteenth century, several rises in POM popularity by P. Souchay starting in the 1940s, M. T. Pope in the 1960s and A. Müller in the 1990s, among many others, have contributed to the development and comprehension of POMs chemistry. Recent times have been especially prolific, with

a steady growth in the number of papers per year, and more than 4,000 items referenced under the topic 'polyoxometalates' by the Web of Science in the last 20 years.

From the theoretical side, POMs are fascinating and have attracted our interest since mid 1990s because of the beauty of their symmetric structures, the presence of multiple metal atoms, their properties and related fascinating phenomena. As this account will show below, describing the molecular and the electronic structure, redox and spectroscopic properties, and reactivity of such species in a proper manner is nowadays feasible, but it was a real challenge 20 years ago.

The first Hartree–Fock LCAO-SCF single point calculation on a polyoxometalate structure was published by M. Bénard, M. M. Rohmer and co-workers in 1991 [14–16], using the Asterix program that had just been developed to suite the particularities of the Cray-1 supercomputer. On Christmas Day, 1989, the Cray-1 installed in the Supercomputer Center of Lausanne (Switzerland) was entirely reserved to compute the SCF wavefunction for the decavanadate anion, $[V_{10}O_{28}]^{6-}$, a relatively large inorganic molecule with high symmetry (D_{2h}). From the room control of the supercomputer, Marie Madeleine Rohmer personally supervised that 10-h-long run. It is worth mentioning that the average cost of a Cray-1 was between \$5,000,000 and \$8,000,000. Nowadays, a home PC processor can get a peak performance of more than 100 GFLOP ($\sim$300 times faster than a Cray-1). The results obtained not only demonstrated how powerful the new computational algorithm was but also opened the way to theoretically analyse the electronic structure of POMs. By using the molecular electrostatic potential and the laplacian of the electron density, the basicity of the different oxygen sites was investigated for the first time. This benchmarking work was followed by a series of pioneering studies on the analysis of Lindqvist and Keggin anions and with host–guest interactions, which were reviewed in 1998 [17].

Ever since, many POMs' features have been tackled by means of computational tools: basicity, NMR chemical shifts, spectroscopy, magnetism, redox properties, solution dynamics, reactivity, etc. (some examples can be found in Refs. [18–25]). Different computational approaches are applied to maximize the accuracy/time ratio. Quantum mechanical calculations have dominated the theoretical publications on POMs during the last two decades, mainly based on density functional methods (DFT), which are moderately time-consuming though accurate enough for providing information on the geometry and the electronic structure. Among the publications devoted to this topic, most focused on the classical Lindqvist $[M_6O_{19}]$, Anderson-Evans $[XM_6O_{24}]$, Keggin $[XM_{12}O_{40}]$, Wells–Dawson $[X_2M_{18}O_{62}]$ and Preyssler $[XP_5W_{30}O_{110}]$ clusters (see Fig. 1), either containing one type of metal ions (W, Mo, V) or a mixture of them. Correlated ab initio calculations (CASSCF/CASPT2 and DDCI) have also been applied to systems containing unpaired electrons, with the goal of unravelling electron (de)localization and spin orientation features [26], electronic energy gaps [27, 28], or to estimate

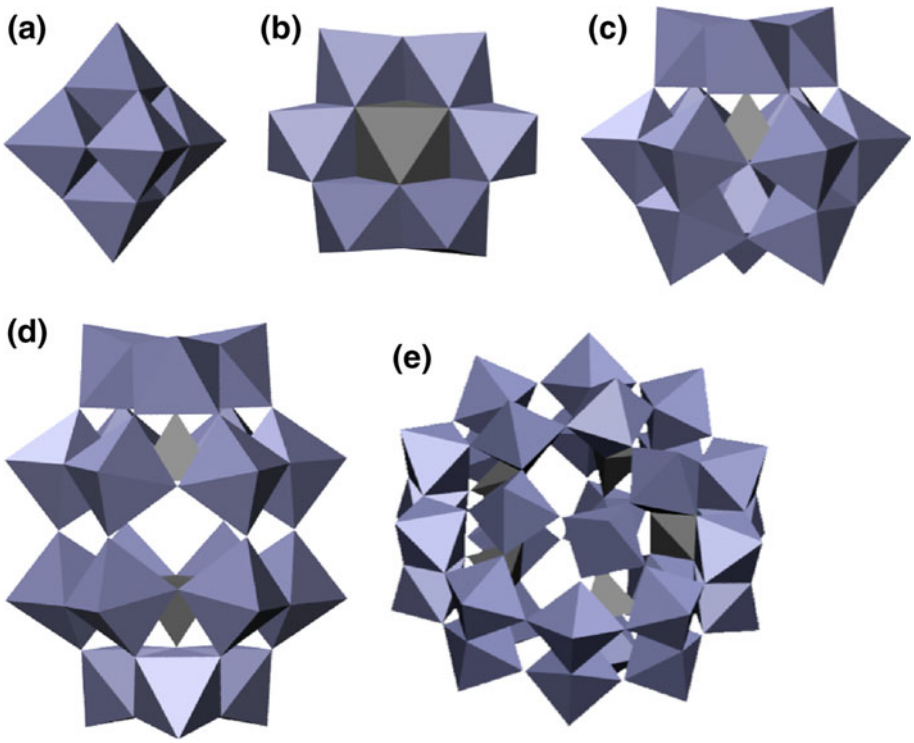

Fig. 1 Polyhedral representation for several typical isopoly-and heteropolyanions: **a** Lindqvist, $[M_6O_{19}]$; **b** Anderson-Evans, $[XM_6O_{24}]$; **c** Keggin, $[XM_{12}O_{40}]$; **d** Wells–Dawson, $[X_2M_{18}O_{62}]$ and **e** Preyssler, $[XP_5W_{30}O_{110}]$. Polyhedral units in *grey* contain the heteroatom, *blue* octahedra represent MO_6 units

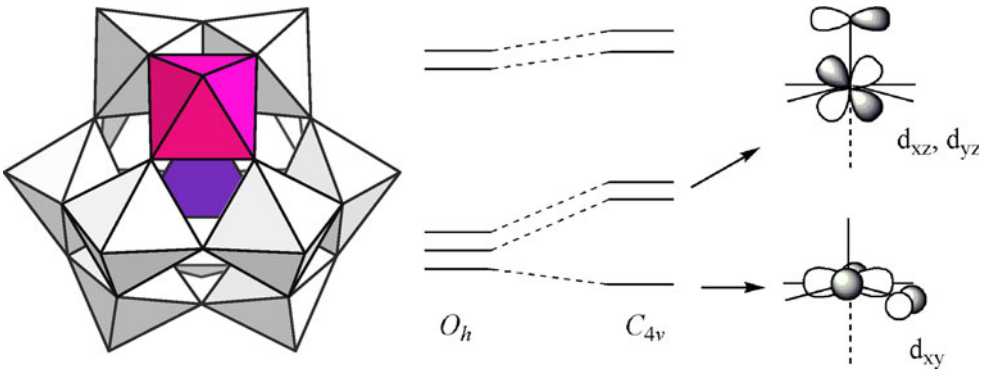

Fig. 2 Polyhedral view of the Keggin anion and MO_6 orbital splitting from O_h to C_{4v} local symmetry. One octahedron is shown in magenta, displaying the connectivity with vicinal polyhedra [31]

local magnetic couplings [29]. These accurate methods are much more time-consuming and thus cannot be routinely applied to large systems, but to the smallest POM members or just to fragments. On the opposite side of computational requirements, we find classical molecular dynamics methods, much more approximate but very useful to study the POMs properties in liquid media such as the interactions with counterions present in solution, or ion pairing processes. A very recent work shows water clustering inside giant POM structures [30]. These calculations are very promising for future research related to self-assembly and supramolecular applications.

Theoretical chemistry in Spain has a long-time tradition that is reflected in the good quality and quantity of the work published in the last 10 years. The scientific contribution of this area includes a rich variety of theoretical methodologies and programme development. Research on POMs carried out by means of computational methods has been also fruitful as the present mini-review shows. We sketch the most relevant work carried out by the Tarragona group (URV, ICIQ) during the last decade. The topics that are discussed concern structural and electronic properties, NMR chemical shifts, redox chemistry, formation process, ion pairing and reactivity. The next future will surely bring interesting and abundant research in this area.

2 Structure, electronic properties and ^{183}W NMR chemical shifts

The basic structural motif common to all POM clusters is the metal oxide MO_n unit, either octahedral (MO_6) or square pyramidal (MO_5). In the most typical octahedral unit, four oxo ligands are bridging to neighbouring octahedra, whereas in apical positions there are a terminal oxygen and an internal one, the latter weakly bound to the metal. The MO_6 unit undergoes a local distortion from the ideal O_h symmetry owing to the packing of several of these units, the actual local point-group symmetry being close to C_{4v}. Because of the symmetry reduction from O_h to C_{4v}, the metal orbitals split from two $\left[\left(d_{xy}, d_{xz}, d_{yz}\right) + \left(d_{x^2-y^2}, d_z^2\right)\right]$ to three $\left[\left(d_{xy}\right) + \left(d_{xz}, d_{yz}\right) + \left(d_{x^2-y^2}, d_z^2\right)\right]$ subsets of orbitals [31], as shown in Fig. 2. In typical POMs, the metal d valence orbitals are empty for M = W^{VI} and Mo^{VI}. Classical fully oxidized POMs without paramagnetic ions present an occupied set of orbitals (or *oxo band* in the literature) well separated from the lowest virtual orbitals (*metal band*). The most stable of the virtual set, or LUMO, is very important from the physicochemical point of view since it governs, to a large extent, the redox processes of POMs and some other properties (catalysis, magnetism, etc.). The computational characterization of the LUMO (composition, localization or delocalization, energy) is thus critical for a successful description of the properties of a POM compound.

POMs based on tungsten or molybdenum are much more common than others due to their optimal relation between charge and size, known to be critical in the high stability of molecular metal oxide aggregates [32]. Polyoxotungstates have larger HOMO–LUMO (H–L) gaps than homologous molybdates, the difference being approximately 0.8 eV for Keggin compounds. As observed from DFT calculations, the nonbonding d(M)–p(O) interactions are dominating the region of frontier orbitals. Such poor covalent interactions between metals and oxo ligands explain why POMs are considered strongly ionic structures. In addition, they are very strong acids despite their high negative charges. On the origin of these unique characteristics is the low surface charge density that can be attributed to a strong inward polarization. Very important also is the fact that electron reduction in most POM clusters is quite innocent from the structural point of view. In single-addenda classical compounds (Keggin, Wells–Dawson), some reductions can be performed without appreciable geometrical changes.

For Dawson structures, this difference between H–L gaps is smaller since the $[P_2Mo_{18}O_{62}]^{6-}$ system displays the alternating bond length (ABL) distortion. ABL has been observed in polyoxomolybdates for a long time, but just recently a theoretical explanation has been proposed [33]. The net effect upon the structure converts the quasi-symmetric O–Mo–O bonds into unbalanced O···Mo–O in a

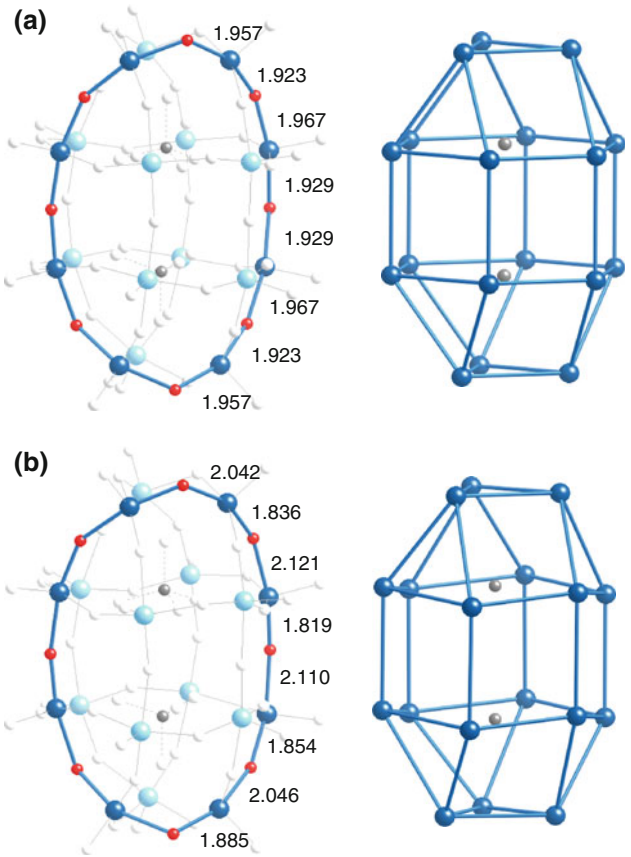

Fig. 3 DFT-optimized geometries for $[P_2Mo_{18}O_{62}]^{6-}$ in **a** hypothetical undistorted D_{3h} and **b** distorted D_3 forms. *Left-hand* views show one Mo_8O_8 loop with selected Mo–O distances in Å (with molybdenum and oxygen in *blue* and *red*, respectively). The rest of the structure is displayed in *soft* colours. To the *right*, only the Mo_{18} frameworks are shown to account for the distortion suffered in the D_3 form [33]

concerted way, displacing the Mo ions off the centre of each octahedron (Fig. 3). The vibronic coupling takes place between a vibrational normal mode and an electronic transition (pseudo Jahn–Teller effect), giving rise to minima in the potential energy surface. So, for the species featuring ABL distortion, it exists an imaginary frequency that indicates the way into which the cluster distorts. Among the cases studied theoretically, it is worth showing that for the symmetrical (O_h) $[Mo_6O_{19}]^{2-}$ Lindqvist anion, a triply degenerate normal mode with imaginary frequency $81i$ cm^{-1} indicates that this structure is not a minimum. In contraposition, the octahedral $[W_6O_{19}]^{2-}$ structure shows an analogous normal mode at 112 cm^{-1} that corresponds to a minimum in the potential energy surface. From an alternative point of view, ABL distortions may be related to the energy gaps observed between frontier orbitals (with metal–oxygen nonbonding π character) in molybdate structures. Calculations show that, upon distortion, the occupied orbitals get more Mo–O π bonding and the unoccupied ones more Mo–O π antibonding, with a net stabilization of the system. Taking the undistorted structures and then comparing them with the fully distorted ones, it can be seen that smaller HOMO–LUMO gaps in undistorted forms produce larger π-orbital mixing and, thus, larger ABL distortion.

Since the preliminary studies on small molecules [34], the theoretical determination of ^{183}W NMR chemical shifts in polyoxtungstates has found serious difficulties [35, 36]. ^{183}W NMR chemical shifts of polyoxotungstates strongly depend on the composition of the medium such as concentration, ionic strength, pH and solvent resulting in 10-ppm deviation of the observed resonance lines [32]. Typically, DFT calculations of polyoxotungstates using Slater TZP basis sets and the BP86 functional give usual deviations of 0.05 Å in some computed bond distances, which is insufficient if we wish to reproduce ^{183}W NMR properties [37]. Our group has shown that the calculation of ^{183}W NMR chemical shifts in polyoxotungstates requires a preliminary computational effort to determine excellent geometries for the anion. This can be achieved using very large basis sets of QZ4P and taking into account the solvent effects [38]. From optimal geometries determined at BP/QZ4P/COSMO, the ^{183}W NMR chemical shifts were computed with the more standard basis sets of TZP quality and including spin–orbit corrections with the ZORA approximation to describe the relativistic effects of the internal electrons. With this strategy, the average deviation from experimental values was found to be about 7 ppm, which is similar to the experimental error. For the family of α-$[XW_{12}O_{40}]^{q-}$ Keggin anions with X belonging to groups 12–15, NMR chemical shifts were computed at different levels of accuracy. The geometry optimization using all electron basis sets of QZ4P quality contracts slightly the distorted WO_6 octahedra, significantly improving the computed chemical shifts. As shown previously, the inclusion of spin–orbit corrections is also fundamental to obtain accurate shieldings for tungsten NMR chemical shifts. For a series of nine Keggin anions, a mean absolute error of 9.3 ppm was reached when the chemical shifts were computed with the above-mentioned methodology. Finally, when the chemical shift is measured in an organic solvent there is a slight expansion of the WO_6 moiety, which shifts the signal approximately 5–10 ppm to more positive values.

3 Redox properties

One of POMs' most investigated features is the ability to reversibly accept and release electrons. This is the basis of catalytic applications, among others. Most POMs get reduced at weakly negative or even slightly positive

potentials, indicating that their empty metal orbitals are low in energy. The high oxidation number of metal ions present in such clusters explains this tendency. From the computational point of view, the modelling of redox potentials has been a challenge in the past decade. However, it is done quite routinely nowadays applying the COSMO [39–41], a numerical method that mimics the solvent effects and that stabilizes the anionic clusters and, thus, their molecular orbitals. Without the solvent effects, there is no match between computed and experimental reduction potentials because the cluster's orbitals are too high in energy. The COSMO incorporates not only the stabilizing effects of the solvent but also those coming from the presence of the counterions in the liquid media that are present to balance the anion negative charge. The solvation effects have been studied in the Keggin anion. The configurations of the solvent molecules were taken from molecular dynamics simulations and included into a quantum mechanics calculation. The first solvation shell was treated explicitly, the electrostatic bulk effect was included modelling 9,000 water molecules as point charges and, finally, the counterions were included as a charge distribution from the radial distribution functions (Fig. 4). The three shells stabilize the POM orbitals but only when all the effects are included, the orbitals have energy comparable with that provided by the COSMO [42]. One of the evidence that the COSMO is able to correctly describe the relative POMs' orbital energies is the electron transfer reaction between $[PW_{12}O_{40}]^{3-}$ and $[P_2W_{18}O_{62}]^{6-}$. As computed in gas phase, the smaller negative charge of the Keggin anion removes the electron off the more charged Dawson anion. However, in solution, the Dawson recovers the electron since its LUMO is correctly placed below in energy with respect to the Keggin partner [43].

POM sizes range from a few metal atoms to giant clusters. These inorganic systems are anionic in nature, and their tendency to accept electrons depend on the negative charge, but also on the size [37]. These two variables act oppositely upon reduction. How do they balance? A comprehensive DFT study showed that the ratio between the molecular charge and the number of metal centres, *q*/*m*, which correlates with the molecular charge density in a simplistic way, explains the propensity of regular POM clusters to accept electrons. For example, the highly charged $[P_2W_{18}O_{62}]^{6-}$ Dawson anion is a stronger oxidant than $[W_4Nb_2O_{19}]^{4-}$.

Different metal addenda atoms can be combined into a single structure to give the mixed-addenda compounds. Their properties depend on the particularities of each metal present, and thus the overall molecular features can be tuned. Many cases have been studied from the computational side. Substitution of a tungsten ion by vanadium produces a more oxidant species. The orbitals of V^V are lower in energy than those of W^{VI}. Similarly, when from a single-addenda tungstate we introduce a Mo^{VI} ion, the final product is also more oxidant. This tunability of the redox properties can also arise from isomerism. Some POM structures present several rotational isomers that display slight variations in the frontier orbitals' energies. In Keggin anions, the most stable α form (T_d) has a LUMO 0.18 eV higher than that of the β form (C_{3v}). The β form is formally produced upon a 60° rotation of a W_3O_{13} triad about a threefold axis of the α form. Both isomers are similar in energy, but reduction is easier in the β form. After the second reduction, a stability inversion occurs and the β isomer gets more stable. The other three rotational isomers of the Keggin anion (γ, δ and ε) were theoretically studied to show that the energy of the LUMOs governs their ability to accept electrons [44].

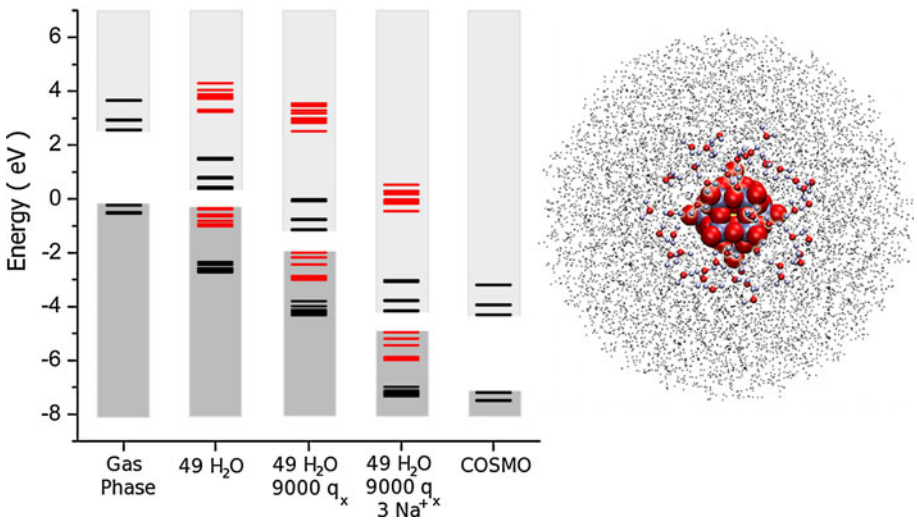

Fig. 4 Energies for the highest occupied and lowest empty levels for different POM–water models. *Black* levels of the Keggin anion; *red* levels of the water molecules; *dark grey* occupied levels; *light grey* empty levels. The *right-hand* view shows the Keggin anion surrounded by explicit water: the first solvation sphere and the point charges [42]

4 Formation

In spite of the extensive theoretical research done in the field of POMs during the last decades, [37, 45–49], only few studies were devoted to analyse their formation mechanisms. Kepert, in the early sixties, suggested that formation of isopolyanions might involve the addition of WO_4 tetrahedra. The first step would imply the addition of a WO_4 unit, acting as a bidentate ligand, to a second WO_4 by expanding the coordination number of the latter metal ion to six [50]. In the late seventies, Tytko and Glemser proposed elaborate mechanisms to explain the formation of POMs based on the addition already formulated by Kepert [51]. There is, however, little experimental evidence to support these mechanisms and some of them do not even agree with experiments [32].

Recently, mechanisms for the nucleation of the Lindqvist anion $[W_6O_{19}]^{2-}$ have been put forward by Poblet and Cronin in a collaborative work that combines theoretical predictions and experiments of electrospray ionization mass spectrometry (ESI–MS) [52]. They use two complementary computational methodologies: (1) standard DFT methods with inclusion of the solvent as a continuum by means of the COSMO model; and (2) Car-Parrinello MD simulations with explicit solvent molecules. In this study, the dinuclear structure proposed by Kepert as the first step of the nucleation process is *not* found to be stable. Other dinuclear structures in which the W^{VI} ions are four- or fivefold coordinated are, however, predicted to be stable. Car-Parrinello MD simulations show that the coordination sphere of W^{VI} ions might be expanded due to direct interaction with water molecules (see Fig. 5). This effect is more important at low pH conditions [53].

Two formation mechanisms have been postulated to justify the clusters that are observed in the ESI–MS fragmentation experiments: $[WO_3(OH)]^-$, $[W_2O_7]^{2-}$, $[W_2O_6(OH)]^-$, $[W_3O_{10}]^{2-}$, $[W_3O_9(OH)]^-$, $[W_4O_{13}]^{2-}$, $[W_4O_{12}(OH)]^-$, $[W_5O_{16}]^{2-}$, $[W_6O_{19}]^{2-}$ and $[W_6O_{18}(OH)]^-$. The aggregation of each $[WO_3(OH)]^-$ monomer is followed by the condensation of a water molecule, with or without previous protonation, as shown in the next lines for the first steps of one of these mechanisms:

$$[WO_3(OH)]^-_{(aq)} + [WO_3(OH)]^-_{(aq)} \rightarrow \left[W_2O_6(OH)_2\right]^{2-}_{(aq)} \quad (1)$$

$$\left[W_2O_6(OH)_2\right]^{2-}_{(aq)} \rightarrow [W_2O_7]^{2-}_{(aq)} + H_2O_{(aq)} \quad (2)$$

$$[W_2O_7]^{2-}_{(aq)} + [WO_3(OH)]^-_{(aq)} \rightarrow [W_3O_{10}(OH)]^{3-}_{(aq)} \quad (3)$$

$$[W_3O_{10}(OH)]^{3-}_{(aq)} + H_3O^+_{(aq)} \rightarrow [W_3O_{10}]^{2-}_{(aq)} + 2H_2O_{(aq)} \quad (4)$$

The structural features and the relative energies of different possible intermediates in such a formation process have been also analysed [54]. An energetic cascade profile is predicted for the two mechanisms with the last steps being the most exothermic. As far as the structural aspects are concerned, a planar W_3 unit is found to be very stable. These W_3 units, which are also observed in clusters with higher nuclearities and even in the Lindqvist anion, act as structural *building blocks* conferring high stability to the intermediate clusters. Those penta- and hexanuclear clusters that most resemble the Lindqvist anion are within the most stable intermediates. In summary, the complementarity between theory and experiment provides important clues about the formation steps of the Lindqvist anion. Further analogous experimental and theoretical work on other iso- and heteropolyanions will provide new insight to accomplish the ambitious purpose of rationalizing such nucleation mechanisms.

5 Ion pairing

Ion pairing is invoked as a ubiquitous effect that orchestrates a variety of processes occurring in several areas of science, including POM chemistry [55]. It is well known that the formation of ion pairs in solution is directly related to a numerous physicochemical properties like redox properties [56], supramolecular chemistry [57], catalytic activity [58] and nuclear magnetic resonance spectra [59]. Traditionally, computational chemists have been focused in

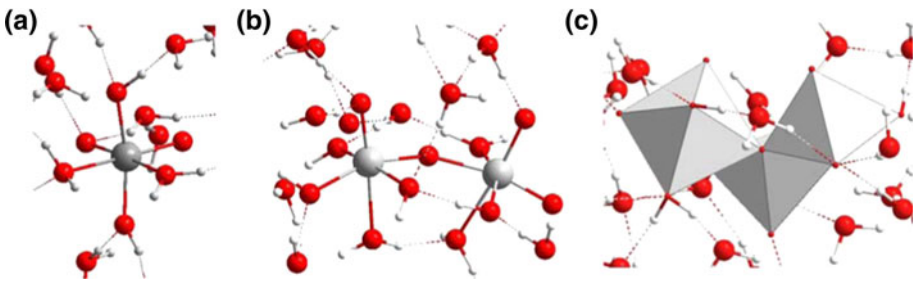

Fig. 5 Representations of the structures for mononuclear (**a**, ball-and-stick), dinuclear (**b**, ball-and-stick) and trinuclear species (**c**, polyhedral) showing the expansion of the coordination sphere of the W(VI) ions due to interaction with the solvent (water). Tungsten in *grey*, oxygen in *red* and hydrogen in *white* [52]

the study of POMs electronic structure and reactivity [37], but in the recent years the first theoretical studies about ion pairing of these species have been reported. In the first part of this section, we will describe some properties of a solution formed by Keggin anions, alkaline ions and water as solvent, whereas in the second part we will show that some giant polyoxometalates like $[H_3Mo_{57}V_6(NO)_6O_{183}(H_2O)_{18}]^{21-}$ can capture counterions over its external surface.

5.1 Keggin anion

The Keggin anion is one of the most relevant members of the POM family with general formula $[XM_{12}O_{40}]^{n-}$ where X and M can be a main-group element (P, Si, Al…) and a transition metal (W, Mo, V…), respectively [32]. By using an electrochemical methodology, Pope and Varga obtained the diffusion coefficients and the hydrodynamic radius (R_H) of $[PW_{12}O_{40}]^{3-}$ and $[SiW_{12}O_{40}]^{4-}$ anions [60]. These authors reported that R_H was invariant under the exchange of different cations in pure water. Grigoriev reported that R_H varies in a series of vanadium monosubstituted Keggin anions, $[XVW_{11}O_{40}]^{n-}$, in water/*tert*-butyl-alcohol (TBA) [61]. It was then concluded that ion pairing was effective in that water–alcohol mixture while it was not in pure water. Moreover, recently $[AlW_{12}O_{40}]^{5-}$ received the attention as a well-behaved model for investigating an outer-sphere electron transfer process in water [62]. Furthermore, it has been shown that mono-valent cations catalyse anion–anion electron transfer reactions [63], and the catalytic effect was explained by the presence of partially dehydrated cations.

Recently, we investigated the structure and the effects on the diffusion coefficient of the ion pairs between $[XW_{12}O_{40}]^{n-}$ anions (X = P, Si, Al; $n = 3, 4, 5$) and mono-valent alkali counterions (Li^+, Na^+, K^+) in water by molecular dynamics simulations [64]. The radial distribution functions of $[PW_{12}O_{40}]^{3-}$ with Na^+ revealed two peaks located at 7.7 Å and 9.9 Å from the centre of the POM (Fig. 6). The first peak has been identified as a contact ion pair between the Na^+ cations and the terminal oxygens of the POM. The second peak has been assigned to a solvent-shared ion pair, in which a water molecule is in between the cation and the terminal oxygen. The substitution of the phosphorous heteroatom by silicon and aluminium increases the POM negative charge and consequently the formation ion pairs as shown in Fig. 6.

Replacement of Na^+ cations by Li^+ affects drastically the ion pair structures previously presented since the solvation shell is more strongly bound around Li^+ cations. Consequently less charged species strongly favours the solvent-shared ion pair structure and, when the charge is increased, this structure collapses to a permanent contact ion pair between the cation and a terminal oxygen.

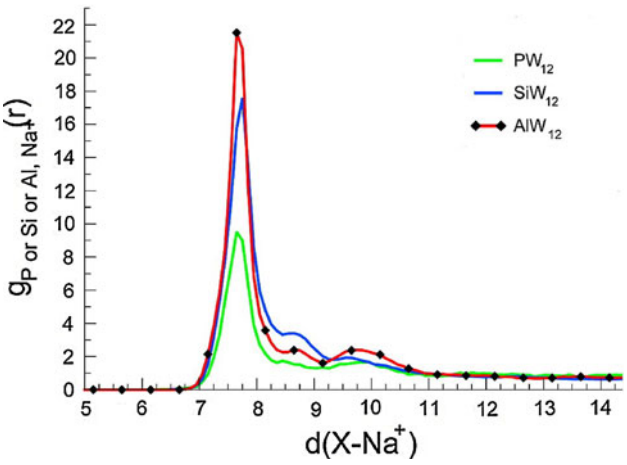

Fig. 6 Radial distribution function (RDF) for the X–Na^+ pair in the $[PW_{12}O_{40}]^{3-}$ (PW_{12}), $[SiW_{12}O_{40}]^{4-}$ (SiW_{12}) and $[AlW_{12}O_{40}]^{5-}$ (AlW_{12}) systems, plotted versus the X–Na^+ distance (in Å) [64]

The computed diffusion coefficients reproduce reasonably well the order of magnitude of the experimental data for similar systems under slightly different conditions [25]. Moreover, the behaviour of the diffusion coefficients does not follow a simple pattern with respect to the heteroatom or countercation in the system. Furthermore, the representation of the diffusion coefficient versus the structural R_H computed from the molecular dynamics simulations unveils a full correlation among them as the Einstein-Stokes equation states.

5.2 Giant polyoxometalates

In the POM field, Liu and Müller realized a long time ago that some POMs do not exist as single ions in water or in other polar solvents [65]. Instead, they tend to further aggregate into nanometric spherical vesicles, called *blackberries*. These supramolecular structures range from 20 to 100 nm in water and consist in a monolayer of thousands of individual POMs with a massive enclosed volume occupied by solvent molecules. Liu unveiled the driving force behind the self-assembly of these vesicles by zeta potential analysis [8]. This technique revealed that the average charge density on each POM unit in blackberries is significantly lower than in the "free" POMs. This experimental evidence suggests that the small counterions are closely associated with, or even incorporated into, the *blackberry* structures acting as glue between the POMs units. The formation of ion pairs also reduces the negative charge of POMs, favouring the growth of *blackberries*.

In collaboration with Müller, we studied the distribution of the countercations (Li^+ and Na^+) on the surface of $[H_3Mo_{57}V_6(NO)_6O_{183}(H_2O)_{18}]^{21-}$ in water by molecular dynamics simulations [66]. This POM was experimentally

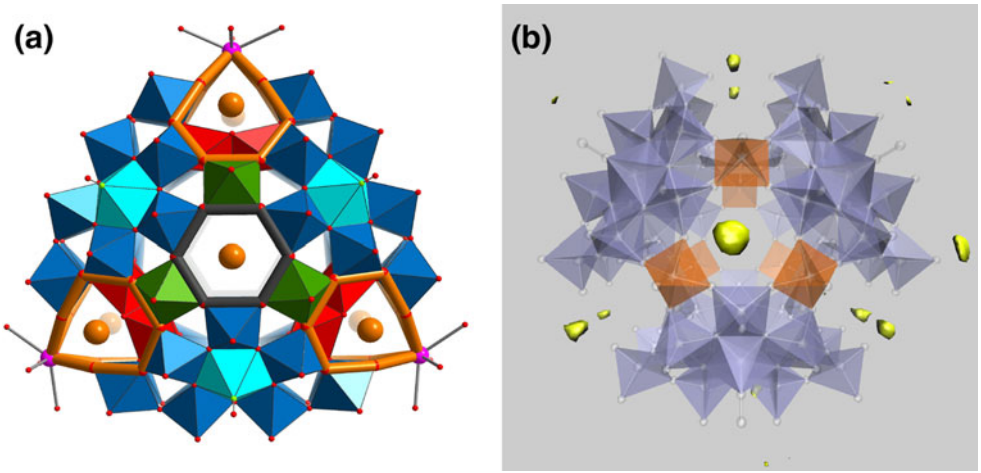

Fig. 7 **a** Polyhedral and ball-and-stick representation (coordinated cations) of $Mo_{57}V_6$. Oxygen in *red*, molybdenum in *blue*, potassium in *pink* and nitrogen in *orange*. **b** Spatial distribution function isosurface of Li^+ counterions around $Mo_{57}V_6$, computed from classical molecular dynamics simulations. The *yellow* isosurface volumes enclose the highest probability regions of finding the cations. Molybdenum framework is shown in *ice blue* and vanadium centres are in ochre [66]

synthesized with a mixture of K^+ and NH_4^+ as counterions [67]. The position of the cations in the crystal structure was determined, revealing a selective complexation of the cations in the pores and external cavities. In one hand, $Mo_3V_3O_6$ pores and the VMo_4O_6 crown-ether type rings interact with NH_4^+. In the other hand, K^+ cations interact with the lateral cavities, closing the VMo_4O_6 rings (Fig. 7a).

In both systems, the spatial distribution function (SDF) reveals two positions of high probability with respect to the cations: at the entrance of the two $Mo_3V_3O_6$ pores and at the VMo_4O_6 lateral cavities (Fig. 7b). Li^+ counterions have a stronger interaction with the pores and the cavities than Na^+ ones, as their probability remains even if the temperature is increased. These positions are in agreement with the ones determined experimentally by X-ray spectroscopy. Additionally, the cations SDF in $Mo_{57}V_6$ demonstrate the interaction between the giant POMs and their cations in water. These computational results suggest the POM–counterion association as the main driving force in the *blackberries* self-assembly.

The cation release/uptake was studied from DFT calculations for a series of X^{n+} cations encapsulated inside a Preyssler anion. Notable energy barriers, ranging from 40 kcal mol^{-1} for Na^+ to 50 kcal mol^{-1} for Th^{4+}, were computed for ion release (E_{out} in Fig. 8). The energy cost for the cation uptake (E_{in}) mainly depends on the dehydration energy of each X^{n+} since the necessary loss of the solvation sphere is a very endothermic process, explaining the high temperatures necessary for the encapsulation of the most charged cations. The energy uptake was estimated to be more than 200 kcal $mol^{-1}$for Th^{4+} [49].

6 Reactivity

One of the most outstanding applications of POMs is catalysis. Because of their properties as strong Brønsted acids and as fast reversible multielectron oxidants, they are applied in acid catalysis and in green selective oxidation with molecular oxygen and hydrogen peroxide. They can also act as bifunctional (acid and redox) catalysts, which make them promising compounds in the field of water oxidation for the utilization of solar energy to obtain molecular oxygen. There are still relatively few theoretical studies on this field, but during last years an increasing number of reports are appearing in the literature. Here, we will summarize the studies carried on two important reactions.

6.1 Water oxidation for energy systems

The recent discovery of the first all-inorganic water oxidation catalyst has bring together the water oxidation and the POM fields [68, 69]. A tetraruthenate core $[Ru_4(\mu\text{-}OH)_2(H_2O)_4]^{6+}$ is stabilized by two γ-$[SiW_{10}O_{36}]^{8-}$ POM ligands. The catalyst mimics the natural oxygen-evolving centre, as the Ru_4 core evolves through four states namely S_n where n is the number of protons and electrons lost (Fig. 9).

We investigated computationally the evolution of the water oxidation catalyst along S_0–S_4 states [70]. The DFT calculations predict a singlet as the most stable multiplicity for the initial S_0 state that is in agreement with the absence of signals in S_0 EPR spectrum. The release of one electron and one proton generate one Ru^V–OH moiety, and the doublet S_1 state is predicted in agreement with the EPR experiments. The rRaman spectrum of S_2 state demonstrates the absence of any $Ru^{VI} = O$ moiety; moreover, the relative position of the second Ru^V–OH moiety with respect to the previously generated one derives in the formation of two *cis–trans* isomers. The *cis* isomer is only 2 kcal mol^{-1} more stable than the *trans* form; consequently, they can be considered degenerate. The S_3 state is a quartet with three Ru^V–OH centres and displaying a clear signal in the EPR spectrum.

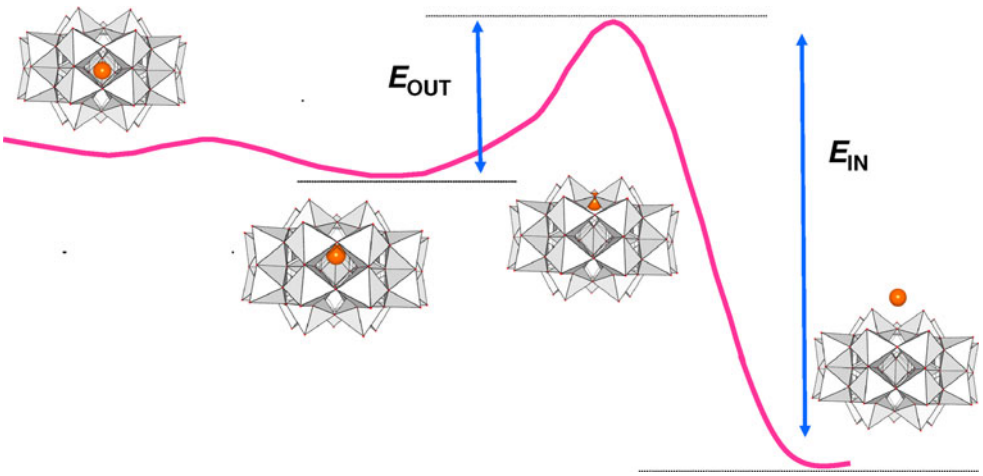

Fig. 8 Schematic energy profile associated with X^{n+} cation (*orange sphere*) release/uptake in a Preyssler anion, $[XP_5W_{30}O_{110}]^{q-}$ [77]

Finally, the active water splitting species with four Ru^{V}–OH centres is achieved. This species is EPR silent in agreement with the calculated singlet ground state. The absence of a S_4 rRaman spectrum does not indicate the absence of isomers with $Ru^{VI} = O$ and Ru^{IV}–H_2O moieties in the S_4 state. Moreover, these species are more than 10 kcal mol^{-1} higher in energy compared with the tetraruthenate core with four Ru^{V}–OH moieties.

The intra- and intermolecular water splitting mechanisms are forbidden due the rigidity of the tetraruthenate core and the first-order reaction rate with respect to the catalyst, as shown by calculations. The molecular orbitals analysis on the catalyst in the S_4 state reveals a high contribution of the Ru^{V}–OH moieties in the LUMO, postulating a nucleophilic attack of a water molecule as the most plausible mechanism.

The rRaman spectrum of the catalyst in the 250–600 cm^{-1} region is sensitive to the evolution of the Ru_4 core. According to our calculations in S_0 state, the low wavenumber bands are assigned to Ru^{IV}–(H_2O) stretching modes (250–400 cm^{-1}), while the prominent feature at 456 cm^{-1} is associated with the normal modes of the Ru_4O_6 core. The new absorptions observed at approximately 500 cm^{-1} in S_1–S_4 rRaman spectra have been assigned to the normal modes of Ru^{V}–OH moieties. The rRaman rationalization is in agreement and demonstrates that in each step through S_0–S_4 states, the catalyst releases one proton and one electron.

Recently, Bonchio has joined the Ru_4 catalyst with sensitizers able to capture light and transfer electrons in order to regenerate the catalyst from S_4 to S_0 state [71–73].

6.2 H_2O_2-based epoxidation

Several theoretical studies have been reported for green H_2O_2-based epoxidations by different types of polyoxometalates: selenium containing dinuclear peroxotungstate $[SeO_4\{WO(O_2)_2\}_2]^{2-}$ [74, 75], lacunary polyoxotungstate

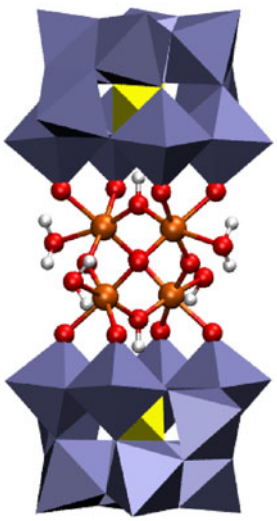

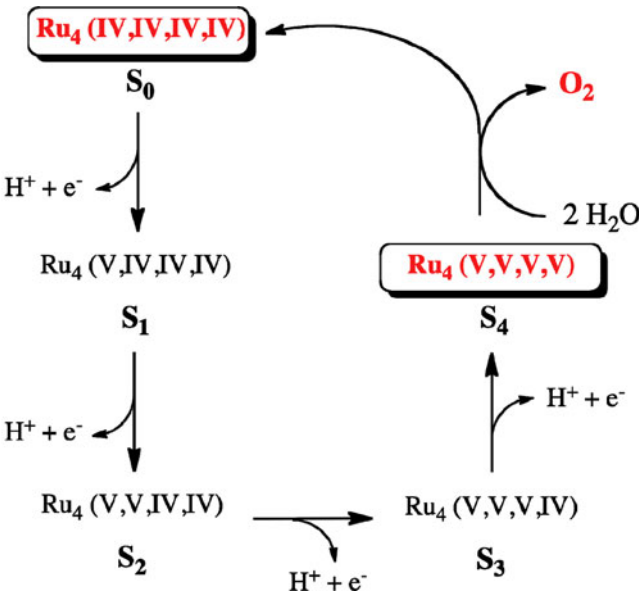

Fig. 9 Structure of the water oxidation catalyst (*left*). γ-$[SiW_{10}O_{36}]^{8-}$ ligands and Ru_4 core in polyhedral in ball-and-stick representation, respectively. Molybdenum in *iceblue*, silicon in *yellow*, oxygen in *red*, hydrogen in *white*, ruthenium in *orange*. Stepwise transformation of the POM-embedded Ru_4 core along S_0–S_4 oxidation states under oxygen-evolving catalysis (*right*) [70]

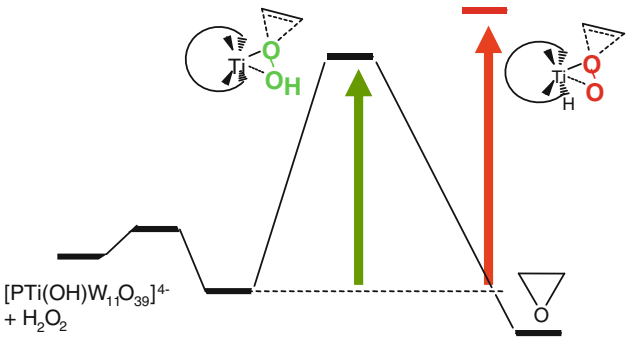

Fig. 10 Schematic energy profile for the ethene epoxidation with H_2O_2 catalysed by $[PTi(OH)W_{11}O_{39}]^{4-}$. The energy barrier for the hydroperoxo mechanism increases when moving from the left to right of the periodic table, whereas the barrier for the peroxo mechanism decreases [78]

$[\gamma\text{-}(SiO_4)W_{10}O_{32}H_4]^{4-}$ [76] and divanadium-substitued polyoxotungstate $[\gamma\text{-}1,2\text{-}H_2SiV_2W_{10}O_{40}]^{4-}$ [22, 77]. Very recently, Antonova et al. [78] studied the epoxidation of alkenes with H_2O_2 by two distinct titanium-substituted POMs $[PTi(OH)W_{11}O_{39}]^{4-}$ and $[Ti_2(OH)_2As_2W_{19}O_{67}]^{8-}$ and compared them with other TM-substituted POMs to assess the effect of the metal nature on the reaction. For both Ti-containing POMs, B3LYP/SMD calculations predict that the Ti-hydroperoxo intermediate is responsible for the oxygen transfer to the alkene to form the epoxide, being the rate-limiting step (see Fig. 10). When we move from left to right and down in the periodic table, the oxygen transfer via peroxo intermediate becomes competitive because of the higher mixing between the orbitals of the transition metal and the O–O unit. Likewise, previous DFT calculations proposed that the Se-containing dinuclear peroxotungstate [74, 75] and γ-V_2-POM follow a peroxo-type mechanism. On the other hand, for lacunary polyoxotungstate Musaev and co-workers discard peroxo mechanism from the interpretation of experimental observations [76].

The $[PTi(OH)W_{11}O_{39}]^{4-}$ and $[Ti_2(OH)_2As_2W_{19}O_{67}]^{8-}$ POMs exhibit a well-defined 6- and 5-coordinated environment, allowing using them as molecular models of Ti single-site catalysts. Thus, several requisites to improve the efficiency of Ti-containing catalysts were proposed: flexible and fivefold (or lower) coordinated Ti environments [78]. Moreover, the higher activity of the Ti_2-POM was attributed to the absence of dimer formation due to the steric shielding of tungsten groups adjacent to Ti centres. The formation of intermolecular linkages between POM units can have important implications not only in catalysis but also in POM assembly to build nano-cluster structures. We investigated the mechanism of dimerization, by acid condensation, between Lindqvist and Keggin anions [79, 80]. The computational studies at BP86/COSMO level revealed that the acid condensation via formation of μ–O linkages is favoured for structures with addendum atoms TM = Ti, Zr and Nb but not for TM = W, Mo and V. Also a correlation between the relative strengths of terminal TM=O bonds and the tendency of these to form dimers was found.

Using pure UBLYP and hybrid UB3LYP functionals, Shaik and co-workers analysed the Mn^{V}=O-based POM intermediate for epoxidation and hydroxylation of alkenes [81] and designed the new Fe^{V}=O catalyst $[Mo_5O_{18}\text{-}Fe{=}O]^{3-}$ as a potential oxidant for monooxygenations [82]. Similarly, with UBP86 functional, we analysed a series of group 6–8 high-valent TM nitrido derivatives $[PW_{11}O_{39}\{TM^{VI}N\}]^{4-}$ and discussed their potential reactivity as nitrogen donor species [24]. The analysis of frontier molecular orbitals allowed rationalizing the observed electrophilic reactivity for the $Ru^{VI}N$ derivative, whose empty antibonding π*(Ru–N) orbitals lay between the oxo and tungsten orbital bands of the POM. Also, calculations showed that the unknown $Mn^{VI}N$ and $Fe^{VI}N$ species could be stabilized by the porphyrin-like ligand $[PW_{11}O_{39}]^{7-}$ and, if it is ever made, should have a high potential reactivity towards nucleophiles.

7 Epilogue

During the last 20 years, computational modelling of polyoxometalates has evolved from the early studies limited at single-point Hartree–Fock level, to the use of bunch of computational techniques that nowadays allow determining a variety of properties and simulating complex phenomena. Because of the anionic nature of the compounds, their computational treatment requires the incorporation of the stabilizing effects of the crystal field in the solid state or of the solvent and the counterions in solution. A definitive step forward was made when solvent effects were taken into account by using continuum methods since these enabled studying their electronic and structural properties and reactivity. Later, the explicit treatment of the solvent and counterions in solution using classical and first-principles molecular dynamics has opened the door to understanding ion pairing, confined water assemblies and nucleation mechanisms among other phenomena.

Theoretical and computational chemists can still find many exciting challenges in the polyoxometalates arena. Some of them are as follows: polyoxometalates deposited over metal and metal oxide surfaces and its implications in material science and heterogeneous catalysis, large nanostructures, the study of nucleation mechanisms of heteropolyanions and large vesicles, the rationalization of cation exchange in polyoxometalates with pores, the reproduction and rationalization of magnetic properties in species with multiple magnetic centres, among many others. Our group

in Tarragona, which has largely contributed to the evolution of the field, will keep working on these and other topics.

Acknowledgments Research supported by the MICINN of Spain (CTQ2008-06549-C02-01/BQU and CTQ2008-06549-C02-02/BQU and Consolider Ingenio 2010 CSD2006-0003), the Generalitat de Catalunya (2005SGR00715, 2009SGR-00462 and XRQTC) and the ICIQ Foundation. Computer resources provided by the BSC-CNS. P.M. thanks the Generalitat de Catalunya for a FI fellowship (2009FIC00026). A.R.F. and X.L. thank the Ramón y Cajal program (RYC-2005-002572 and RYC-2008-02493).

References

1. Pope MT, Müller A (1991) Angew Chem Int Ed 30:34
2. Hill CL (ed) (1998) Chem Rev 98:1
3. Long D-L, Burkholder E, Cronin L (2007) Chem Soc Rev 36:105
4. Long D-L, Tsunashima R, Cronin L (2010) Angew Chem Int Ed 49:1736
5. Wassermann K, Dickman MH, Pope MT (1997) Angew Chem Int Ed 36:1445
6. Müller A, Kögerler P, Kuhlmann C (1999) Chem Commun 1347
7. Kortz U, Hussain F, Reicke M (2005) Angew Chem Int Ed 44:3773
8. Liu G, Liu T, Mal SS, Kortz U (2006) J Am Chem Soc 128:10103
9. Kim G-S, Zeng H, Neiwert WA, Cowan JJ, VanDerveer D, Hill CL, Weinstock IA (2003) Inorg Chem 42:5537
10. Okuhara T, Mizuno N, Misono M (1996) Adv Catal 41:113
11. Neumann R (1998) Prog Inorg Chem 47:317
12. Kozhevnikov IV (2002) Catalysts for fine chemical synthesis, vol 2, Catalysis by Polyoxometalates. Wiley, Chichester
13. Kamata K, Yonehara K, Nakagawa Y, Uehara K, Mizuno N (2010) Nature Chem 2:478
14. Rohmer M-M, Ernenwein R, Ulmschneider M, Wiest R, Bénard M (1991) Int J Quantum Chem 40:723
15. Kempf JY, Rohmer M-M, Poblet JM, Bo C, Bénard M (1992) J Am Chem Soc 114:1136
16. Rohmer M-M, Bénard M (1994) J Am Chem Soc 116:6959
17. Rohmer M-M, Bénard M, Blaudeau J-P, Maestre JM, Poblet JM (1998) Coord Chem Rev 178–180:1019
18. Maestre JM, Sarasa JP, Bo C, Poblet JM (1998) Inorg Chem 37:3071
19. Bardin BB, Davis RJ, Neurock M (2000) J Phys Chem B 104:3556
20. Maestre JM, López X, Bo C, Poblet JM (2002) Inorg Chem 41:1883
21. Suaud N, Gaita-Ariño A, Clemente-Juan JM, Coronado E (2004) Chem Eur J 10:4041
22. Kuznetsov AE, Geletii YV, Hill CL, Morokuma K, Musaev DG (2009) Inorg Chem 48:1871
23. Fernández JA, López X, Poblet JM (2007) J Mol Catal A 262:236
24. Romo S, Antonova NS, Carbó JJ, Poblet JM (2008) Dalton Trans 38:5101
25. López X, Nieto-Draghi C, Bo C, Bonet-Ávalos J, Poblet JM (2005) J Phys Chem A 109:1216
26. López X, de Graaf C, Maestre JM, Bénard M, Rohmer M-M, Bo C, Poblet JM (2005) J Chem Theory Comput 1:856
27. Romo S, de Graaf C, Poblet JM (2008) Chem Phys Lett 450:391
28. de Graaf C, Caballol R, Romo S, Poblet JM (2009) Theor Chem Acc 123:3
29. de Graaf C, López X, Ramos JL, Poblet JM (2010) Phys Chem Chem Phys 12:2716
30. Mitra T, Miró P, Tomsa AR, Merca A, Bögge H, Bonet-Ávalos J, Poblet JM, Bo C, Müller A (2009) Chem Eur J 15:1844
31. Maestre JM, López X, Bo C, Casañ-Pastor N, Poblet JM (2001) J Am Chem Soc 123:3749
32. Pope MT (1983) Heteropoly and isopoly oxometalates. Springer-Verlag, Berlin
33. Yan L-K, López X, Carbó JJ, Sniatynsky R, Duncan DC, Poblet JM (2008) J Am Chem Soc 130:8223
34. Rodríguez-Fortea A, Alemany P, Ziegler T (1999) J Phys Chem 103A:8288
35. Bagno A, Bonchio M, Autschbach J (2006) Chem Eur J 12:8460
36. Gracia J, Poblet JM, Fernández JA, Autschbach J, Kazansky LP (2006) Eur J Inorg Chem 1149
37. Poblet JM, López X, Bo C (2003) Chem Soc Rev 32:297
38. Vilà-Nadal L, Sarasa JP, Rodríguez-Fortea A, Igual J, Kazansky LP, Poblet JM (2010) Chem Asian J 5:97
39. Klamt A, Schüürmann G (1993) J Chem Soc Perkin Trans 2:799
40. Andzelm J, Kölmel C, Klamt A (1995) J Chem Phys 103:9312
41. Klamt A (1995) J Chem Phys 99:2224
42. Miró P, Poblet JM, Bonet-Ávalos J, Bo C (2009) Can J Chem 87:1296
43. López X, Bo C, Poblet JM (2002) J Am Chem Soc 124:12574
44. López X, Poblet JM (2004) Inorg Chem 43:6863
45. Bagno A, Bonchio M (2005) Angew Chem Int Ed 44:2023
46. Duclusaud H, Borshch SA (2001) J Am Chem Soc 123:2825
47. Kumar D, Derat E, Khenkin AM, Neumann R, Shaik S (2005) J Am Chem Soc 127:17712
48. Quinonero D, Wang Y, Morokuma K, Khavrutskii LA, Botar B, Geletii YV, Hill CL, Musaev DG (2006) J Phys Chem B 110:170
49. Fernández JA, López X, Bo C, de Graaf C, Baerends EJ, Poblet JM (2007) J Am Chem Soc 129:12244
50. Kepert DL (1962) Prog Inorg Chem 4:199
51. Tytko KH, Glemser O (1976) Adv Inorg Chem Radiochem 19:239
52. Vilà-Nadal L, Rodríguez-Fortea A, Yan L-K, Wilson EL, Cronin L, Poblet JM (2009) Angew Chem Int Ed 48:5452
53. Rodríguez-Fortea A, Vilà-Nadal L, Poblet JM (2008) Inorg Chem 47:7745
54. Vilà-Nadal L, Rodríguez-Fortea A, Poblet JM (2009) Eur J Inorg Chem 5125
55. Marcus Y, Hafter G (2006) Chem Rev 106:4585
56. Macchioni A (2005) Chem Rev 105:2039
57. Pope MT, Müller A (2001) Polyoxometalate chemistry: from topology via self-assembly to applications. Kluwer Academic Publishers, Netherlands
58. Grigoriev VA, Cheng D, Hill CL, Weinstock IA (2001) J Am Chem Soc 123:5292
59. Vankova N, Heine T, Kortz U (2009) Eur J Inorg Chem 34:5102
60. Pope MT, Varga GM Jr (1966) Inorg Chem 5:1249
61. Grigoriev VA, Hill CL, Weinstock IA (2000) J Am Chem Soc 122:3544
62. Geletii YV, Hill CL, Bailey AJ, Hardcastle KI, Atalla RH, Weinstock IA (2005) Inorg Chem 44:8955
63. Czap A, Neuman NI, Swaddle TW (2006) Inorg Chem 45:5918
64. Leroy F, Miró P, Poblet JM, Bo C, Bonet-Ávalos JB (2008) J Phys Chem B 112:8591
65. Liu TB, Diemann E, Li HL, Dress AWM, Müller A (2003) Nature 426:59
66. Müller A, Sousa FL, Merca A, Bögge H, Miró P, Fernández JA, Poblet JM, Bo C (2009) Angew Chem Int Ed 48:5934
67. Lutz HD, Nagel R, Mason SA, Müller A, Bögge H, Krickemeyer E (2002) J Solid State Chem 165:199
68. Sartorel A, Carraro M, Scorrano G, De Zorzi R, Geremia S, McDaniel ND, Bernhard S, Bonchio M (2008) J Am Chem Soc 130:5006

69. Geletii YV, Besson C, Hou Y, Yin QS, Musaev DG, Quinonero D, Cao R, Hardcastle KI, Proust A, Kogerler P, Hill CL (2009) J Am Chem Soc 131:17360
70. Sartorel A, Miró P, Salvadori E, Romain S, Carraro M, Scorrano G, Di Valentin M, Llobet A, Bo C, Bonchio M (2009) J Am Chem Soc 131:16051
71. Orlandi M, Argazzi R, Sartorel A, Carraro M, Scorrano G, Bonchio M, Scandola F (2010) Chem Commun 46:3152
72. Orlandi M, Argazzi R, Sartorel A, Carraro M, Scorrano G, Bonchio M, Scandola F (2010) Chem Commun 46:3152
73. Puntoriero F, La Ganga G, Sartorel A, Carraro M, Scorrano G, Bonchio M, Campagna S (2010) Chem Commun 46:4725
74. Kamata K, Ishimoto R, Hirano T, Kuzuya S, Uehara K, Mizuno N (2010) Inorg Chem 49:2471
75. Kamata K, Hirano T, Kuzuya S, Mizuno N (2009) J Am Chem Soc 131:6997
76. Prabhakar VR, Morokuma K, Hill CL, Musaev DG (2006) Inorg Chem 45:5703
77. Nakagawa Y, Mizuno N (2007) Inorg Chem 46:1727
78. Antonova NS, Carbó JJ, Kortz U, Kholdeeva OA, Poblet JM (2010) J Am Chem Soc 132:7488
79. López X, Weinstock IA, Bo C, Sarasa JP, Poblet JM (2006) Inorg Chem 45:6467
80. Kholdeeva OA, Maksimov GM, Maksimovskaya RI, Vanina MP, Trubitsina TA, Naumov DY, Kolesov BA, Antonova NS, Carbó JJ, Poblet JM (2006) Inorg Chem 45:722
81. Khenkin AM, Kumar D, Shaik S, Neumann R (2006) J Am Chem Soc 129:15451
82. Derat E, Kumar D, Neumann R, Shaik S (2006) Inorg Chem 45:8655